Satellite Aerosol Composition Retrieval from a combination of three different Instruments: Information content analysis

Ulrike Stöffelmair[1,2], Thomas Popp[1], Marco Vountas[2], and Hartmut Bösch[2]

[1]German Aerospace Center (DLR)
[2]University of Bremen, Institute of Environmental Physics (IUP)

Correspondence: Ulrike Stöffelmair (ulrike.stoeffelmair@dlr.de)

Abstract. This study focuses on the information content for retrieving Aerosol Optical Depth (AOD) and its components from satellite measurements. We utilize an optimal estimation retrieval algorithm with data from three satellite-based instruments: SLSTR on Sentinel 3A/3B, IASI and GOME-2 on Metop A/B/C. Data are averaged to a common 40x80 km^2 grid, temporally aligned within a 60-minute window and cloud masked. A simulation study will be carried out to analyse the information content of the instrument combination, identify retrievable parameters and initiate the development of a uniform retrieval algorithm for the AOD and aerosol components. The simulation study for the information content analysis is implemented using the radiative transfer model SCIATRAN and uses MERRA-2 reanalysis data for AOD and mass mixing ratios of different aerosol components. The study shows 6 to 15 degrees of freedom for the determination of aerosol components dependent on AOD and the underlying surface. The results will be used for the development of a synergistic multi-sensor retrieval algorithm for AOD and its components in cloud-free atmospheres across various surface types.

1 Introduction

Aerosols impact radiation and climate in a multitude of ways and, after CO2, their combined effects are the second largest contributor to the radiative forcing. Due to the complexity of the aerosol-climate effects, aerosols are the largest contributor to uncertainties (Forster et al., 2021; Li et al., 2022).

Their direct, semidirect and indirect effects depend not only on the aerosol abundance and geospatial distribution but also on the aerosol chemical composition (Boucher et al., 2013; Kaufman et al., 2002). Direct radiative effects will lead to warming for strongly absorbing aerosols (e.g. dust, black and organic carbon absorbing aerosols ...) (Matsui et al., 2018; Samset et al., 2018; Kok et al., 2023) whereas for most other aerosols will reduce the radiation and energy input into the atmosphere by reflecting solar radiation and thus have a cooling effect (Charlson et al., 1992; Kaufman et al., 2002; Arias et al., 2021; Li et al., 2022). The indirect effects due to aerosol cloud interactions are due to aerosol particles acting as condensation nuclei for water droplets and nucleating particles for ice crystals in clouds, which depends also on the aerosol composition, because different aerosol components function differently well as condensation nuclei (Twomey, 1974, 1977; Burrows et al., 2022; Seinfeld et al., 2016; Storelvmo, 2017). Other indirect effects are related to changes in surface albedo due to deposited aerosols. An example of the semidirect effect is the uneven distribution of radiative heating in the troposphere caused by aerosols, which

25 leads to atmospheric convection and circulation (Sherwood et al., 2015). All these effects depend on the aerosol composition (Kaufman et al., 2002; Yin et al., 2002; Wiacek et al., 2010; Arias et al., 2021; Forster et al., 2021; Kok et al., 2023). Due to the major effect of aerosols and their composition on the climate, they play a critical role in climate modelling (Myhre et al., 2017; Gliß et al., 2021; Randles et al., 2017). Observational data are important also for those climate models for validation and assimilation purpose. It is not sufficient to have information on AOD and distribution but also composition information

30 is needed if we want to reduce uncertainties of aerosols on climate. Hence, there is an important need for climate research for global monitoring of aerosol components from satellite measurements (Kaufman et al., 2002; Holzer-Popp et al., 2008; Li et al., 2022; Kacenelenbogen et al., 2022).

Typically, the retrieval of AOD from satellite measurements is an ill-posed mathematical inversion problem which limits

35 the capabilities to identify components of the AOD. This means that there are not enough information about aerosols and their composition, other atmospheric parameters such as temperature, pressure or trace gas concentrations and surface in the measurement data. By combining data from different satellite instruments, complementary information, like varying spectral ranges and observation geometries, can be combined (Dubovik et al., 2021b), which holds the potential to improve the capabilities for inferring AOD composition. For this purpose a retrieval algorithm based on optimal estimation (Rodgers, 2000)

40 shall be applied which makes use of data from three different instruments measuring with different observation characteristics, different spectral ranges (ultraviolett (UV), visible (VIS) and thermal infrared (TIR)) and different viewing geometries (nadir and oblique).

Aerosol component retrieval based on passive measuring instruments are best known as SYNAER (Holzer-Popp and Schroedter,

45 1999; Holzer-Popp et al., 2008) and GRASP/Component (Li et al., 2019, 2020; Zhang et al., 2021; Dubovik et al., 2021a). SYNAER works with predefined aerosol mixtures (fixed mixes of different aerosol components), determines these and not individual aerosol components (Holzer-Popp et al., 2008), as in the retrieval planned here. The component retrieval of GRASP works very well based on the multi-axis and polarimetric data from POLDER/PARASOL, whereas we focus on a extended spectral coverage with partly highly spectrally resolved data. Aside from that the POLDER time series extends from 1996 to

50 2013 and is expected to start again in 2025 with 3MI (Fougnie et al., 2018). As we are also interested in current phenomena, the coverage of the last few years is important to us. For these reasons among others, we use the instruments described below. The instruments included are the dual-view radiometer SLSTR (Sea and Land Surface Temperature Radiometer) onboard Sentinel 3A and 3B (Coppo et al., 2010), the Infrared Atmospheric Sounding Interferometer (IASI) (Blumstein et al., 2004) and the spectrometer Global Ozone Monitoring Experiment-2 (GOME-2) (Munro et al., 2006; Callies et al., 2000), both onboard

55 Metop A/B/C.
The SLSTR measurement with nine channels in the VIS and TIR provides additional information due to the two different viewing directions (nadir and oblique) and additional channels in the visible range and provides options for better separation of ground and atmospheric influences. IASI shows greater sensitivity for the detection of mineral dust and larger particles. The measurement in the UV range of GOME-2 provides information about the absorption and thus enables the separation of

60 absorbing and non-absorbing particles.

Due to the partial overlap of the wavelength ranges, the SLSTR measurements can be used to check the spectral consistency of the 3 instruments and thus filter out pixels with changes within the half-hour time offset in the overflight that the two satellites have. The temporal overlap of GOME-2 and IASI (both on METOP A/B/C) is important for the combination of the instruments due to the rapid possible changes in aerosol and cloud distribution and in our case outweighs the advantages that Sentinel 5P,

65 for example, has with a similar wavelength range to GOME-2 but with significantly better resolution. The planned retrieval is designed for the coarsest resolution of the instruments used (GOME-2 with 40kmx80km), on which the other instruments are averaged to.

To analyse the aerosol components for climate research, the longest possible time series is required. This is made possible by the possible use of the predecessor instruments (A)ATSR(2) at SLSTR, GOME and SCIAMACHY at GOME-2 and HIRS at

70 IASI, which provide temporal coverage from 1995 to the present with one interruption (2012 to 2016) (Coppo et al., 2010; Loyola et al., 2009; Inamdar et al., 2023). The selected resolution is sufficiently fine for the planned use of the retrieval for climate studies, while it would be too coarse for regional air quality analyses.

As a first step towards developing this multi-sensor retrieval algorithm a simulation-based information content analysis is presented in this study.

75

There exist aerosol retrieval algorithms exploiting data of single instruments, but they are not retrieving aerosol components. For example, the AOD and the Fine mode AOD can be determined from SLSTR data (Sayer et al., 2010; Bevan et al., 2012; Sogacheva et al., 2017) , the Absorbing Aerosol Index from GOME-2 (Hasekamp et al., 2004) and Dust AOD from IASI (Vandenbussche et al., 2013; Callewaert et al., 2019; Clarisse et al., 2019; Capelle et al., 2014; Klüser et al., 2012). There

80 are also algorithms using a combination of different instruments types to determined more information about the composition for example SYNAER (Holzer-Popp et al., 2008), which uses AATSR (Advanced Along Track Scanning Radiometer) and SCIAMACHY (Scanning Imaging Absorption Spectrometer for Atmospheric Chartography) both on Envisat, predecessor instruments to SLSTR and GOME-2, the OLCI–SLSTR SYNERGY aerosol product (North and Heckel, 2019) combining SLSTR and OLCI (Ocean and Land Color Instrument) on Sentinel 3A and 3B or PMAp (Grzegorski et al., 2021), which uses

85 the polarization channels of GOME-2, IASI and AVHRR (Advanced Very High Resolution Radiometer).

For SYNAER the information content for aerosol type determination is shown to be 2 to 3 degrees of freedom (DGF) for fixed AOD and surface albedo (Martynenko et al., 2010) using a principle component analysis. According to Klüser et al. (2015), depending on the spectral database of optical properties, AOD and dust layer temperature used, values of up to 6.7 pre-

90 vail for the DGF for determining the dust AOD, dust particle size, composition, emission temperature and height. Hasekamp and Landgraf (2005) show that aerosol retrieval based on simulated polarised and unpolarised GOME-2 measurements over the ocean provides 6 to 8 total degrees of freedom calculated with the optimal estimation method, reducing to 3.5 to 5 when only considering the intensity measurements. The determined parameters were the aerosol loading of both modes of the bimodal aerosol size distribution, the effective radius of at least one mode, the refractive index (real and imaginary part), the aerosol

95   layer height and the oceanic pigment concentration.

Consistent with the planned retrieval setup, an information content analysis is performed in this study with simulated cloud-free pixels with realistic observation geometry for the instrument ensemble. A set of observations resembling the above mentioning instruments is simulated with the SCIATRAN radiative transfer model (Rozanov et al., 2014; Mei et al., 2023) for different observing conditions / geometries, surface types, aerosol compositions and aerosol amounts in realistic scenarios. With these

100   data an analysis of the combined information content is then conducted which focuses on capabilities for the determination of aerosol abundance (total AOD) and aerosol components in a cloud-free atmosphere. This analysis uses the Optimal Estimation Theory developed by Rodgers (2000) to calculate the degrees of freedom. This information content analysis will be used to theoretically identify which parameters can be retrieved from the multi-sensor data. It will then be used to develop a synergistic multi-sensor retrieval algorithm for AOD and aerosol components. The planned synergistic retrieval focuses on the determina-

105   tion of the aerosol composition for further investigation of the described climate influences.

This paper starts with a brief theory of information content (Sec. 2) to specify the used definitions. Simulated satellite measurements are used so that the true values are known and are described in Sec. 3. The used methods for the quantitative analysis of the information content is explained in Sec. 4. Section 5.2 presents the results for the information gain and the information content of the instrument combination, which are finally discussed in Sec. 6.

2   Theory of information content and Optimal Estimation

110

The Optimal Estimation theory (Rodgers, 2000, 1996; Maahn et al., 2020) describes the forward model as

$$\mathbf{y} = \mathbf{F}(\mathbf{x}) + \epsilon, \tag{1}$$

where $\mathbf{y}$ represents the observation vector, i.e. the vector which contains the individual measurements in our case the reflectance, $\mathbf{x}$ the state vector, which contains the parameters that will be retrieved, $\mathbf{F}$ the forward model, which is in our case

115   the radiative transfer model SCIATRAN and ϵ is the experimental error including observation noise and forward model uncertainty. In general in Optimal Estimation the cost function is minimised.

We consider a non-linear iterative solution. According to the Bayesian optimal estimation theory from Rodgers the next iteration step $\mathbf{x}_{i+1}$ is calculated with:

$$\mathbf{x}_{i+1} = \mathbf{x}_a + (\mathbf{K}_i^T \mathbf{S}_\epsilon^{-1} \mathbf{K}_i + \mathbf{S}_a^{-1})^{-1} \mathbf{K}_i^T \mathbf{S}_\epsilon^{-1} (\mathbf{y} - \mathbf{F}(\mathbf{x}_i)$$

120

$$+ \mathbf{K}_i(\mathbf{x}_i - \mathbf{x}_a). \tag{2}$$

$\mathbf{x}_a$ is the prior state vector and $\mathbf{S}_a$ the corresponding error covariance matrix. $\mathbf{K}$ is the Jacobian matrix consisting of the partial derivatives of each measurement with respect to each state element ($\mathbf{K}_{ij} = \frac{\partial y_j}{\partial x_i}$).

The posterior error covariance matrix $\hat{\mathbf{S}}$ describes the statistical uncertainties of $\hat{\mathbf{x}}$ due to the errors from observation, forward model assumptions and apriori and is calculated as

125   $$\hat{\mathbf{S}}^{-1} = \mathbf{K}^T \mathbf{S}_\epsilon^{-1} \mathbf{K} + \mathbf{S}_a^{-1} \tag{3}$$

The square root of the diagonals of $\hat{\mathbf{S}}$ represent the 1σ uncertainty of the retrieved parameters. For the information content analysis the averaging kernel matrix

$$\mathbf{A} = \frac{\partial \hat{\mathbf{x}}}{\partial \mathbf{x}} = (\mathbf{K}^T \mathbf{S}_\epsilon^{-1} \mathbf{K} + \mathbf{S}_a^{-1})^{-1} \mathbf{K}^T \mathbf{S}_\epsilon^{-1} \mathbf{K} \tag{4}$$

is used to calculate the Degrees of Freedom (DGF). The total DGF is calculated as

$$\mathrm{DGF}_{\text{total}} = \mathrm{Trace}(\mathbf{A}) = \sum_{i=1}^{n} \mathbf{A}_{ii} \tag{5}$$

and the diagonal elements of $\mathbf{A}$ represent the DGF per element of the state vector $\mathbf{x}$:

$$\mathrm{DGF}_i = \mathbf{A}_{ii} = \frac{\partial \hat{x}_i}{\partial x_i} \tag{6}$$

The values of $\mathbf{A}_{ii}$ are in the range of 0 (no information on x_i) to 1 (x_i can be fully determined) and characterize the sensitivity of each retrieved parameter to its truth. This makes the DGF a good indicator of the number of parameters that can be determined in retrieval.

3 Simulation of Satellite Measurements

For the simulation of satellite measurements the radiative transfer model SCIATRAN (Rozanov, 2022; Rozanov et al., 2014; Mei et al., 2023), is used to simulate the collocated data from the three instruments on common GOME-2 pixels: SLSTR on Sentinel 3-A and 3-B (since 2017), IASI and GOME-2 both on Metop A/B/C (since 2007).

3.1 Radiative transfer forward model

We use SCIATRAN as a forward model for radiative transfer and to create synthetic measurements for this information content study. SCIATRAN simulates radiance spectra appropriate to atmospheric remote sensing observations from UV to TIR spectral range. We calculate the radiance at the top of atmosphere (TOA) using the assumption of a pseudo-spherical atmosphere with the scalar discrete ordinate technique. For the solar spectrum the Thekaekara (NREL; Drummond and Thekaekara, 1973) spectrum is used.

The surface is handled as a Lambertian reflector with wavelength dependent albedo. The wavelength-dependent emissivity of the surface is set to the climatology values measured with IASI since 2008 (Zhou et al., 2011, 2013, 2018, 2021). The influence of aerosols on TOA radiation is calculated using the different aerosol components defined in the MERRA-2 dataset. The optical database in the MERRA-2 model comprise precomputed values for extinction, scattering efficiency, and expansion coefficients of scattering matrix elements at specific wavelengths and humidity levels as well as cross-sectional area and particle mass at predefined humidity levels for 15 aerosol components. These components include hydrophobic and hydrophilic modes of black carbon (BCPHOBIC, BCPHILIC) and organic carbon (OCPHOBIC, OCPHILIC), sulfate (SO4), and five distinct size bins for sea salt (SS001, ..., SS005) and dust (DU001, ..., DU005) aerosols (Randles et al., 2017). The aerosol components are listed with their dry effective radius in Tab. A1.

3.2 Satellite Measurements and Observation Vector

Satellite TOA radiance data for the three instruments are averaged at a common grid of 40×80 km^2 within a temporal matching window of 60 minutes for the planned retrieval. The choice of instruments has been made with the goal that they complement each other in terms of their information content since they measure in different spectral ranges and with different viewing geometries.

A short overview over the instruments, their characteristics and their contribution to the observation vector is listed below.

3.2.1 Sea and Land Surface Temperature Radiometer (SLSTR)

SLSTR measures with the dual-view principle observing the same spot on Earth twice along track in nadir and oblique (rearward) view (55°) and accordingly with two different path lengths through the atmosphere, which enables a better decoupling of the radiation contributions from the ground and the atmosphere (Barton et al., 1989). SLSTR has a swath width of approximate 750km and a spatial resolution of 0.5kmx0.5km in the VIS and SWIR range and 1kmx1km in the thermal range for nadir pixels (Coppo et al., 2010; European Space Agency, 2024). The different measurement channels, listed in European Space Agency (2024) with their central wavelength and bandwidth, are all used in the observation vector with both viewing directions. For the different channels the radiative transfer calculations are performed on an internal wavelength grid and averaged using a rectangular function as a simplification of the spectral response function.

3.2.2 Infrared Atmospheric Sounding Interferometer (IASI)

IASI is a passive infrared Fourier Transform Spectrometer (FTS), which measures in a spectral range from 3.7 to 15.5μm using a Michelson interferometer, and an infrared camera connected to it, which works in the spectral range from 10.3 to 12.5μm. Through an inverse Fourier transformation and radiometric calibration, an interferogram is calculated in the IASI instrument. IASI has a swath width of 2400km. The IASI footprints are circles with about 12km diameter (Blumstein et al., 2004; Hébert et al., 2017; Simeoni et al., 2004).

The precise measurements in the infrared spectral range contain information about the quantity and properties of the dust aerosol particles.

Following Vandenbussche (2021) the observation vector contains IASI data in the original spectral resolution (0.25cm^{-1}) from 8914.6 to 9111.6nm and from 10796.2 to 11061.9nm. For the used Level 1C data a spectral harmonisation removing the impact of instrument spectral response from the radiance spectra (EUMETSAT, 2019).

3.2.3 Global Ozone Monitoring Experiment-2 (GOME-2)

GOME-2 on board of Metop A/B/C is the improved version of the Global Ozone Monitoring Experiment on the second European Remote Sensing Satellite (GOME on ERS-2). GOME-2 is an optical spectrometer with 4096 channels in four bands in the range of $240 - 790$nm with a high spectral resolution of 0.26–0.51nm and a spectral range for each pixel form 0.07 to

6

0.2 (EUMETSAT, 2022). A scan mirror enables across-track scanning in nadir direction with a swath width of 1920km and can also be directed to different calibration sources. It has a footprint of 80km (across-track) x 40km (along-track) (Munro et al., 2016; EUMETSAT AC SAF), which is the driver for the resolution of the study and the planned retrieval.

From GOME-2 the data from 342.33nm to 792.40nm with a wavelength step of approximately 10nm is used in the observation vector. A higher resolution is not necessary because aerosols do not have sharp absorption lines but broad structures (Andersson, 2017).

3.3 State Vector

The state vector analysed for its information content contains the different parameters which shall be inverted in the retrieval algorithm - and to be developed in the future. Those are: surface albedo values at different wavelengths (340nm, 494nm, 555nm, 670nm, 758nm, 868nm, 2500nm), the surface temperature, the AOD at 550nm and the scaling factors for the different 15 aerosol components (Tab. A1). Each provided aerosol component height profile is assumed to be scalable with one parameter, in the following called the scaling factor. The scaling factors are applied to normalized vertical mass mixing ratio profiles, taken from monthly mean MERRA-2 data, to obtain the profile of the aerosol components mass mixing ratio.

3.4 Apriori values used in Optimal Estimation

We use the following data as a priori values for the described parameters of the state vector: For the surface albedo values from 340 to 758nm we use the climatological values of the GOME-2 surface LER database (Tilstra et al., 2017, 2021) for the geographical position. For the albedo values at 868nm and 2500nm, we set the a priori values to 0.2 and 0.15, as we do not have any climatological values here. The a priori value of the surface temperature is set to 295K. For the AOD and the scaling factors of the aerosol components, the monthly mean values from MERRA-2 data (Global Modeling And Assimilation Office and Pawson, 2015a, b) are used.

4 Method for quantitative analysis of the information content

In this study we use the Optimal Estimation theory, described in Sec. 2, and the pyOptimalEstimation package (Maahn et al., 2020) to calculate the information content for aerosol retrieval from the combination of three instruments. To work with realistic aerosol composition and AOD values in the simulated scenarios we use MERRA-2 data for AOD (Global Modeling And Assimilation Office and Pawson, 2015a) and mass mixing ratios of the different aerosol components (Global Modeling And Assimilation Office and Pawson, 2015b).

The mass mixing ratios are re-gridded from $0.5°\times0.625°$ to $1°\times1°$ using bilinear interpolation. The satellite overpasses are at 9:30 am for the Metop satellite, with GOME-2 and IASI on it, and 10:00 am for Sentinel 3A and 3B, with SLSTR on board. So we select for each timezone, every 3 hours in the MERRA-2 data, the nearest to 9:30 am local solar time. These data are then used to calculate monthly means. The daily and monthly vertical mass mixing ratio profiles are then normalized to 1kgkg^{-1}. The scaling factors to reconstruct the original daily vertical profiles are used for the simulation study. Those scaling factors are

applied to the normalized monthly profiles for the creation of mass mixing ratio files for the radiative transfer calculations. The relative humidity is taken from MERRA-2.

220 We use solar angles calculated with the python package pvlib (Anderson et al., 2023) at a local solar time of 9:30 am which corresponds to the satellite overpasses. For the satellite viewing geometry, we use the case that all instruments measure as close as possible near nadir above the point under consideration. That means 0° viewing zenith angle for GOME-2 and IASI and 6° for the nadir view of SLSTR.

For the surface albedo the GOME-2 surface LER climatology data (Tilstra et al., 2017, 2021) is used as a priori information.
225 The instrument errors, S_y, 2% for GOME-2 (EUMETSAT, 2005), 5% for the SLSTR radiance channels and 0.5K for the infrared channels from SLSTR (European Space Agency, 2024) and for IASI (Vandenbussche, 2021), are taken into account in the calculation of the DGFs.

5   Results and Analysis

In order to consider a representative range of all parameters global scenarios based on the MERRA-2 reanalysis are used.
230 To analyse the gain in information content (Sec. 5.1) of the instrument combination compared to the individual instruments, the data of the 1st, 15th and 30th of the middle months of each season (January, April, July and October) of the year 2018 are used. These are regridded using nearest neighbour interpolation from the 1°x1° grid to a 10°x10° grid in order to consider the best possible coverage of different aerosol compositions with a reduced amount of data. This results in 6948 simulated scenarios for each individual instrument and for the combination.
235 For the more detailed analysis of the information content of the instrument combination (Sec. 5.2), we use data from the 15th of January, April, July and October on the 1°x1° grid. This larger dataset, 231805 simulated scenarios for this consideration, also allows us to recognise patterns on global maps of degrees of freedom.

5.1   Increase in information content through the combination of instruments

240 To analyse the increase in information content from the combination of instruments compared to the individual instruments, we use 6948 simulated scenarios designed like specified in Sec. 4.

The analysis of the total DGF shows a clear gain in information from the total degrees of freedom of the individual instruments ranging from 5 to 8 for GOME-2, from 8 to 13 for SLSTR and from 4 to 10 for IASI up to 14 to 20 DGF by combining the instruments, as shown in Fig.1.
245 The degrees of freedom of the aerosol components, defined as the total sum of the DGF for all aerosol components, are more crucial for the primary goal of determining the aerosol composition. A clear gain in information content is also evident here - from 1 to 6 for GOME-2, 3 to 12 for SLSTR and 2 to 10 for IASI to 6 to 15 for the combination of instruments, as can be seen in Fig. 2.
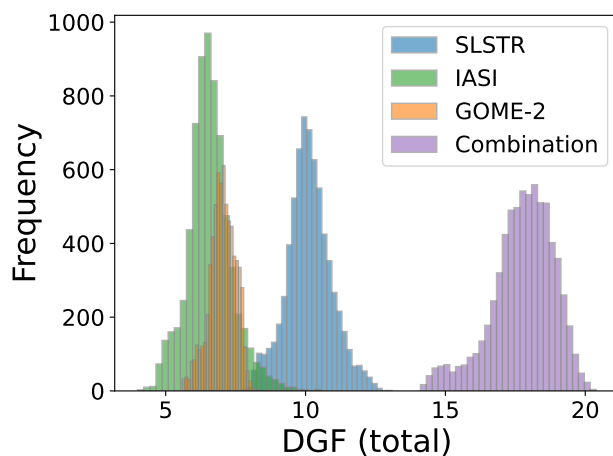
Figure 1. Histogram showing the distribution of the total DGF for the individual instruments (SLSTR in blue from 8 to 13, GOME-2 in orange from 5 to 8 and IASI in green from 4 to 10) and for the combination of these instruments in purple from 14 to 20.
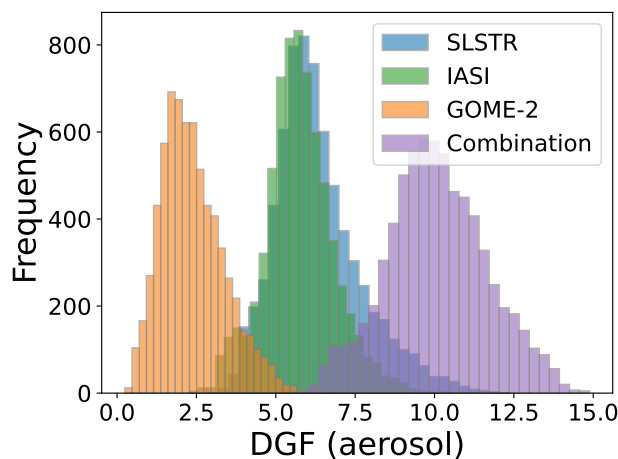

Figure 2. Histogram showing the distribution of the sum of DGF for the aerosol components for the individual instruments (SLSTR in blue from 3 to 12, GOME-2 in orange from 1 to 6 and IASI in green from 2 to 10) and for the combination of these instruments in purple.

This increase in information content through the combination of these three instruments shows that complementary information adds up to a more detailed picture of the aerosol properties in the atmosphere. This proves the potential for the planned aerosol retrieval to allow retrieving information on the aerosol composition, i.e. their contributions to total AOD.

9

5.2 Information content analyses for the combined datasets

Analyzing the information content of data gridded at a higher spatial resolution (1°x1°) for only the 15th of each month reveals the following correlations. They show that an increase in the degrees of freedom for aerosol component determination can be
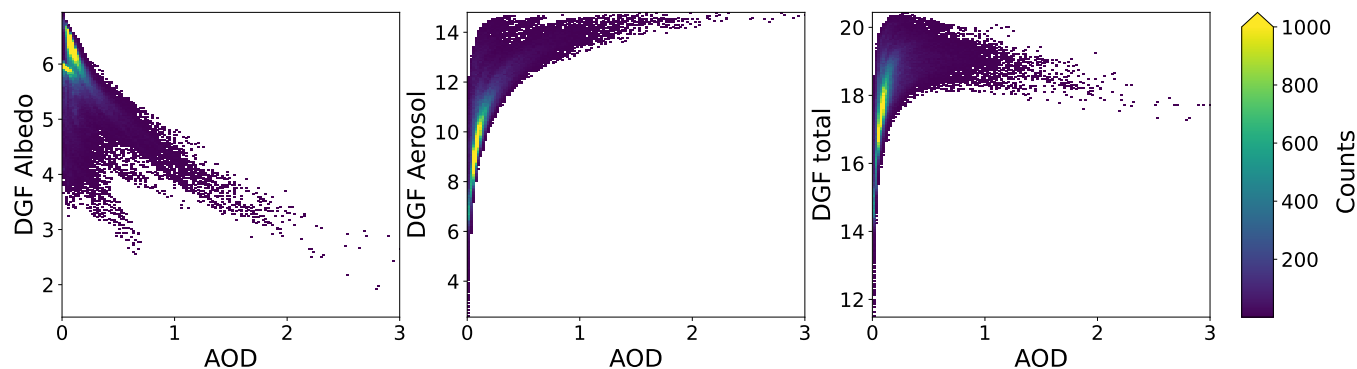

Figure 3. 2D histogram showing the relationship between the total DGF (left), the DGF for the aerosol components (center) and the DGF for albedo (right) and the AOD.

255   observed following a logarithmic-shape function with increasing AOD, see Fig. 3 center. This means that with a higher aerosol load, more aerosol components can be separated from each other. This is consistent with the results of e.g. Martynenko et al. (2010); Hasekamp and Landgraf (2005); Hou et al. (2017). When considering the degrees of freedom used to determine the surface albedo as a function of AOD, an opposite behaviour is observed - a decreasing number of degrees of freedom for the spectral albedo determination with increasing AOD, as can be seen in Fig. 3 right. The determination of surface albedo becomes

260   more difficult at higher aerosol loading, because of the shielding effect of aerosols, which is well known and is described for example in Köpke (2012); Popp (1995). For the total degrees of freedom, there is also a logarithmic increase up to approx. $AOD = 0.3$, which turns into a slow linear decrease at higher AOD values, see Fig. 3 left. This behaviour can be well explained as a combination of the two contributing pieces for aerosol and surface information.

265   As an example the maps in Fig. 4 depict the distribution of the total DGF (top left), the DGF of the aerosol components (top right), the DGF of the albedo retrieval (lower left) and the AOD (lower right) at the 15th of July. It is obvious that in areas with high aerosol amounts (such as over the Sahara and over the Atlantic within the Sahara dust plume), more degrees of freedom are identified for the determination of aerosol components. Also, over the Roaring Forties and Furious Fifties between 40° and 60° S higher DGFs for the determination of aerosol components appear which are probably related to the higher concentration

270   of larger sea salt aerosol components near their source regions. In contrast, we see an opposite effect with similar spatial pattern when considering the degrees of freedom for albedo determination.
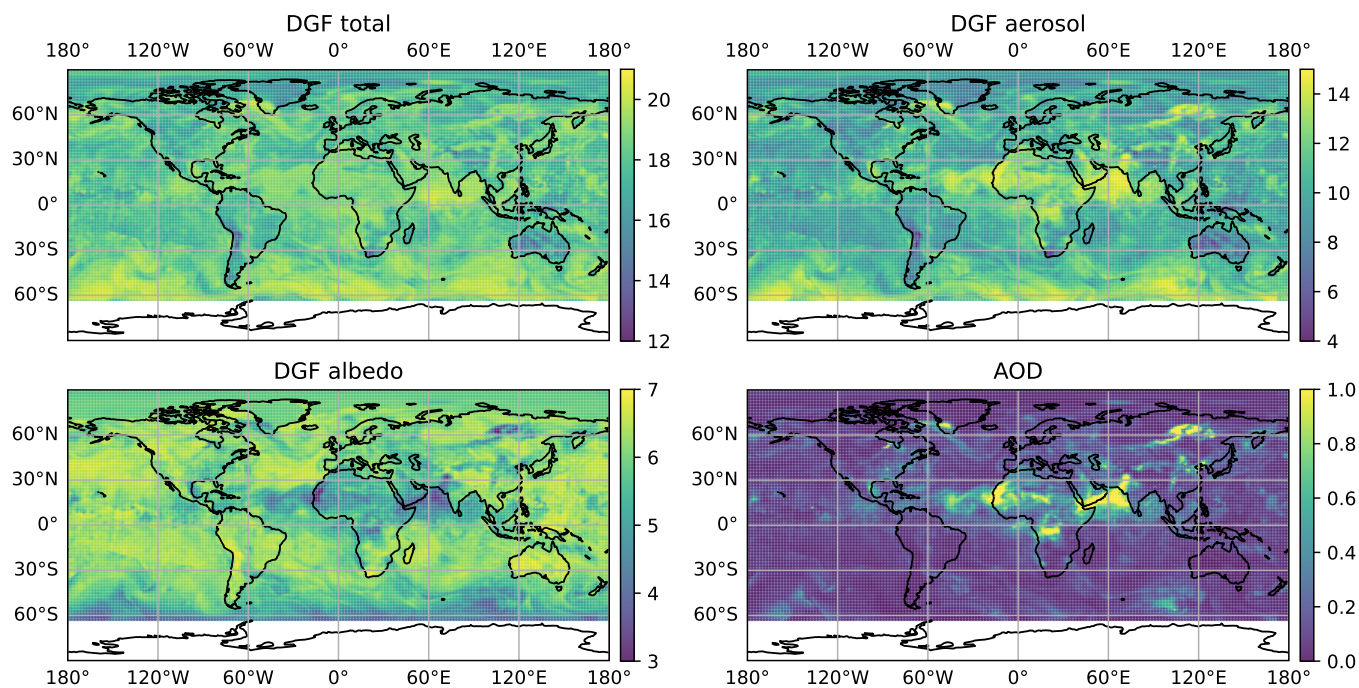
Figure 4. Maps showing the distribution of total DGF (top left), DGF for aerosol components (top right), DGF for albedo (down left) and the AOD (down right) on 15.07.2018.
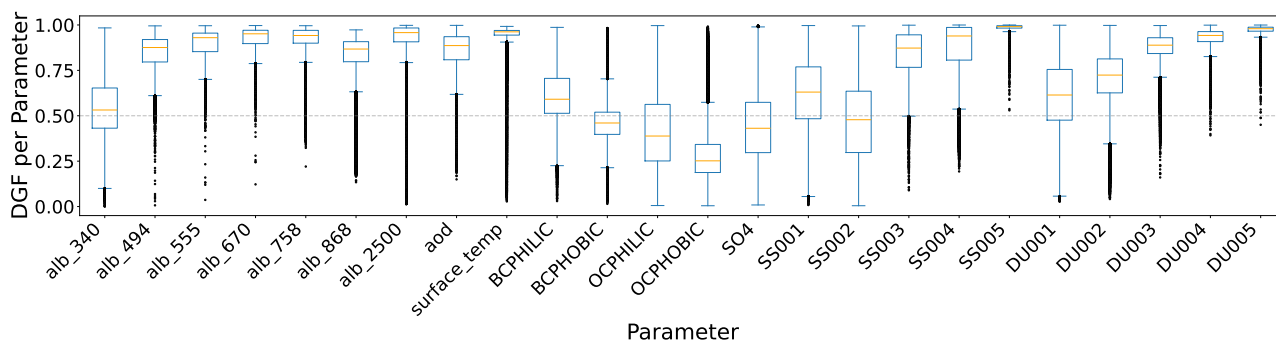

Figure 5. Boxplot showing the distribution of DGF values per parameter within all simulated scenarios. A value above 0.5 (dashed grey line) means that this parameter can be retrieved well. The orange line shows the median, the blue box contains the values between the lower and upper quartile, the whiskers indicate the minimum and maximum values and if the whiskers are longer than 1.5 times the box, all values exceeding this range are labelled as outliers in black.

The observation of higher DGF for aerosol components over areas with large sea salt or dust aerosol fraction at comparatively low total AOD is also supported by Fig. 5. There we take a closer look at the degrees of freedom for the individual parameters, shown as boxplots from all 231805 simulated scenarios in Fig. 5, the capability for determination of the individual parameters

275

11

can be identified. A value larger than 0.5 (above the dashed grey line) means that this parameter can be determined well (Hou et al., 2018). The spectral albedo values, the surface temperature and the AOD can be determined quite well. When analysing the aerosol components, it is clearly visible that larger particles (e.g. sea salt and dust from bin 003) can be determined reliably in more cases. In the case of carbon compounds, the quantity of hydrophilic aerosols can be determined more frequently than
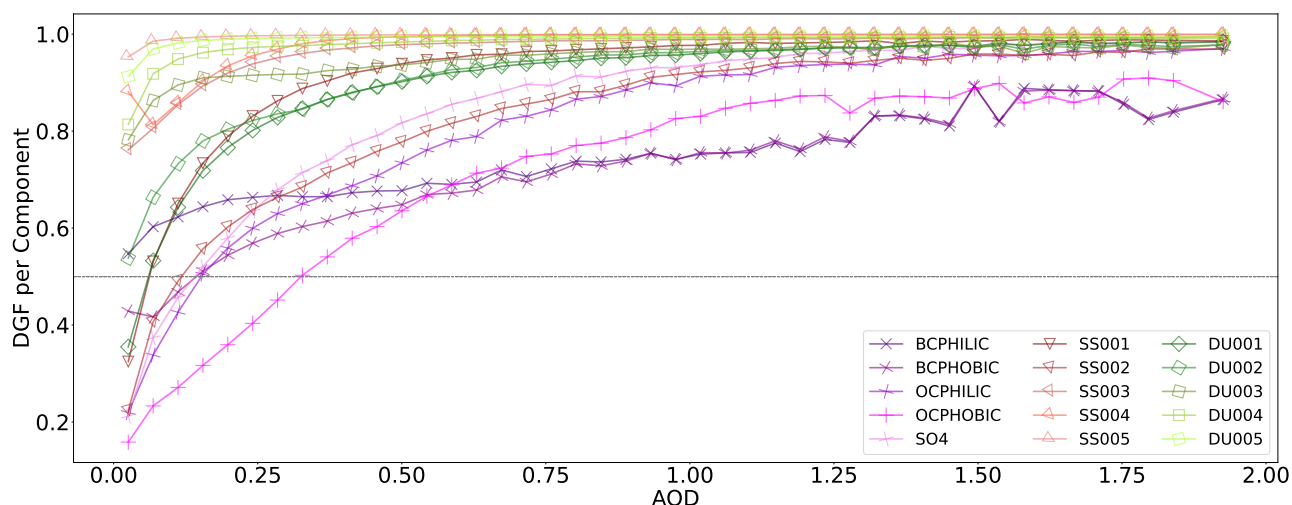
280   hydrophobic aerosols.

Figure 6. Mean values of the binned data of the degrees of freedom per aerosol component plotted against total AOD. The underlying 2D histograms with bin means and standard deviations are shown in A1.

These findings are further supported by Fig. 6 where the different DGFs per aerosol component are plotted against the total AOD. When examining the degrees of freedom of dust and sea salt particles, an increase is observed with rising AOD, asymptotically approaching the value 1.With increasing particle size, a higher initial value at low AOD and a more rapid increase can be observed. The fine mode aerosol components also show an increase in the degrees of freedom with increasing AOD. However, black carbon aerosols show a less pronounced increase than the organic carbon aerosols and sulphates, with black carbon also exhibiting a higher DGF value of 0.45 (hydrophobic) and 0.55 (hydrophilic) at low AOD compared to organic carbon and sulphate with a value of approximate 0.2. Also, the black carbon saturation levels remain well below 1.

290   The observations of Fig. 5 and Fig. 6 thus show a higher retrieval capability with increasing AOD and with increasing particle size as well as with decreasing absorption in the fine mode.

6 Discussion and Conclusion

In this paper we have analysed the information content for an aerosol retrieval using a combination of the three instruments SLSTR on Sentinel 3A and B, GOME-2 and IASI both on METOP A/B/C and the information gain coming from this combi-

295 nation as compared to the individual sensors. The information gained by combining the three instruments for aerosol retrieval was clearly shown and is important for further climate studies.

From the simulation study, it can be concluded that in addition to at best 7 spectral surface albedo values, the surface temperature and total AOD, the sensor combination offers the possibility of determining the mass mixing ratios for 6 to 15 aerosol components and thus also their contribution to the AOD. The number of parameters that can be determined depends both on the

300 AOD (more parameters can be determined with a higher AOD) and on the soil type. How well the aerosol components can be determined also depends on the particle size. This means that the mass mixing ratios of aerosol components can be determined more easily with larger particle sizes.

The DGF analysis incorporated realistic measurement noise values (the diagonal elements of the measurement error co-

305 variance matrices) for all instruments, but did not include potential error correlations between the channels (the off-diagonal elements of the measurement error covariance matrices). Additionally, true retrieval will face several issues which may reduce DGF values i.e. vaying time shifts between the 2 satellites, different viewing angle constellations and calibration inconsistencies / biases between the instruments.

310 The results presented here show the capabilities to determine spectral ground albedo as well as AOD and the aerosol composition of up to 15 components by combining the data of the three instruments. This is a significant gain in information compared to single-sensor aerosol retrievals. Those currently used single-sensor aerosol retrievals can usually determine total AOD and fine mode AOD, or dust AOD alone, and ground albedo at one wavelength; best instruments (multi-angle polarimeters such as POLDER) allow to invert AOD, fine mode AOD and single scattering albedo (Holzer-Popp et al., 2013). Retrieving more in-

315 formation on aerosol composition opens up further scientific analysis of aerosol-related geophysical phenomena, for example, the transport of desert dust or of aerosols caused by forest fires, due to their occurrence outside their source regions, but also from industrial combustion and the impact of Covid-19 related restrictions on emissions from industry and the transport sector. A more detailed separation of aerosol components will also enable further research into direct aerosol effects on the climate system and into aerosol-cloud interactions and associated indirect effects on regional radiative forcing.

320 **Appendix A: DGF aerosol components**

Table A1. Aerosol components used for this study from MERRA-2 (Randles et al., 2017).

Aerosol Component	abbreviation	dry effective radius in μm
Dust Bin 1	DU001	0.64
Dust Bin 2	DU002	1.34
Dust Bin 3	DU003	2.32
Dust Bin 4	DU004	4.20
Dust Bin 5	DU005	7.75
Sea Salt Bin 1	SS001	0.08
Sea Salt Bin 2	SS002	0.27
Sea Salt Bin 3	SS003	1.05
Sea Salt Bin 4	SS004	2.50
Sea Salt Bin 5	SS004	7.48
Hydrophobic Black Carbon	BCPHOBIC	0.04
Hydrophilic Black Carbon	BCPHILIC	0.04
Hydrophobic Organic Carbon	OCPHOBIC	0.09
Hydrophilic Organic Carbon	OCPHILIC	0.09
Sulfate	SO_4	0.16

analysis. MV developed the idea of using MERRA-2 data to get realistic aerosol compositions in the simulations and helped US to integrate them. US develop the code for the study with support of MV. All authors conceived the research and significantly contributed to the scientific

325 discussions.

References

Anderson, K. S., Hansen, C. W., Holmgren, W. F., Jensen, A. R., Mikofski, M. A., and Driesse, A.: pvlib python: 2023 project update, Journal of Open Source Software, 8, 5994, https://doi.org/10.21105/joss.05994, 2023.

Andersson, A.: A Model for the Spectral Dependence of Aerosol Sunlight Absorption, ACS Earth and Space Chemistry, 1, 533–539, https://doi.org/10.1021/acsearthspacechem.7b00066, 2017.

Arias, P., Bellouin, N., Coppola, E., Jones, R., Krinner, G., Marotzke, J., Naik, V., Palmer, M., Plattner, G.-K., Rogelj, J., Rojas, M., Sillmann, J., Storelvmo, T., Thorne, P., Trewin, B., Rao, K. A., Adhikary, B., Allan, R., Armour, K., Bala, G., Barimalala, R., Berger, S., Canadell, J., Cassou, C., Cherchi, A., Collins, W., Collins, W., Connors, S., Corti, S., Cruz, F., Dentener, F., Dereczynski, C., Luca, A. D., Niang, A. D., Doblas-Reyes, F., Dosio, A., Douville, H., Engelbrecht, F., Eyring, V., Fischer, E., Forster, P., Fox-Kemper, B., Fuglestvedt, J., Fyfe, J., Gillett, N., Goldfarb, L., Gorodetskaya, I., Gutierrez, J., Hamdi, R., Hawkins, E., Hewitt, H., Hope, P., Islam, A., Jones, C., Kaufman, D., Kopp, R., Kosaka, Y., Kossin, J., Krakovska, S., Lee, J.-Y., Li, J., Mauritsen, T., Maycock, T., Meinshausen, M., Min, S.-K., Monteiro, P., Ngo-Duc, T., Otto, F., Pinto, I., Pirani, A., Raghavan, K., Ranasinghe, R., Ruane, A., Ruiz, L., Sallée, J.-B., Samset, B., Sathyendranath, S., Seneviratne, S., Sörensson, A., Szopa, S., Takayabu, I., Tréguier, A.-M., van den Hurk, B., Vautard, R., von Schuckmann, K., Zaehle, S., Zhang, X., and Zickfeld, K.: Technical Summary, pp. 35–144, Cambridge University Press, https://doi.org/10.1017/9781009157896.002, 2021.

Barton, I. J., Zavody, A. M., O'Brien, D. M., Cutten, D. R., Saunders, R. W., and Llewellyn-Jones, D. T.: Theoretical algorithms for satellite-derived sea surface temperatures, Journal of Geophysical Research: Atmospheres, 94, 3365–3375, https://doi.org/10.1029/jd094id03p03365, 1989.

Bevan, S. L., North, P. R., Los, S. O., and Grey, W. M.: A global dataset of atmospheric aerosol optical depth and surface reflectance from AATSR, Remote Sensing of Environment, 116, 199–210, https://doi.org/10.1016/j.rse.2011.05.024, 2012.

Blumstein, D., Chalon, G., Carlier, T., Buil, C., Hebert, P., Maciaszek, T., Ponce, G., Phulpin, T., Tournier, B., Simeoni, D., Astruc, P., Clauss, A., Kayal, G., and Jegou, R.: IASI instrument: technical overview and measured performances, https://doi.org/10.1117/12.560907, 2004.

Boucher, O., Randall, D., Artaxo, P., Bretherton, C., Feingold, G., Forster, P., Kerminen, V.-M., Kondo, Y., Liao, H., Lohmann, U., Rasch, P., Satheesh, S., Sherwood, S., Stevens, B., and Zhang, X.: Clouds and Aerosols, Cambridge University Press, 2013.

Burrows, S. M., McCluskey, C. S., Cornwell, G., Steinke, I., Zhang, K., Zhao, B., Zawadowicz, M., Raman, A., Kulkarni, G., China, S., Zelenyuk, A., and DeMott, P. J.: Ice-Nucleating Particles That Impact Clouds and Climate: Observational and Modeling Research Needs, Reviews of Geophysics, 60, https://doi.org/10.1029/2021rg000745, 2022.

Callewaert, S., Vandenbussche, S., Kumps, N., Kylling, A., Shang, X., Komppula, M., Goloub, P., and De Mazière, M.: The Mineral Aerosol Profiling from Infrared Radiances (MAPIR) algorithm: version 4.1 description and evaluation, Atmospheric Measurement Techniques, 12, 3673–3698, https://doi.org/10.5194/amt-12-3673-2019, 2019.

Callies, J., Corpaccioli, E., Eisinger, M., Hahne, A., and Lefebvre, A.: GOME-2-Metop's second-generation sensor for operational ozone monitoring, ESA Bull., 102, 28–36, 2000.

Capelle, V., Chédin, A., Siméon, M., Tsamalis, C., Pierangelo, C., Pondrom, M., Crevoisier, C., Crepeau, L., and Scott, N. A.: Evaluation of IASI-derived dust aerosol characteristics over the tropical belt, Atmospheric Chemistry and Physics, 14, 9343–9362, https://doi.org/10.5194/acp-14-9343-2014, 2014.

Charlson, R. J., Schwartz, S. E., Hales, J. M., Cess, R. D., Coakley, J. A., Hansen, J. E., and Hofmann, D. J.: Climate Forcing by Anthropogenic Aerosols, Science, 255, 423–430, https://doi.org/10.1126/science.255.5043.423, 1992.

Clarisse, L., Clerbaux, C., Franco, B., Hadji-Lazaro, J., Whitburn, S., Kopp, A. K., Hurtmans, D., and Coheur, P.: A Decadal Data Set of Global Atmospheric Dust Retrieved From IASI Satellite Measurements, Journal of Geophysical Research: Atmospheres, 124, 1618–1647, https://doi.org/10.1029/2018jd029701, 2019.

375 Coppo, P., Ricciarelli, B., Brandani, F., Delderfield, J., Ferlet, M., Mutlow, C., Munro, G., Nightingale, T., Smith, D., Bianchi, S., Nicol, P., Kirschstein, S., Hennig, T., Engel, W., Frerick, J., and Nieke, J.: SLSTR: a high accuracy dual scan temperature radiometer for sea and land surface monitoring from space, Journal of Modern Optics, 57, 1815–1830, https://doi.org/10.1080/09500340.2010.503010, 2010.

Drummond, A. and Thekaekara, M.: The Extraterrestrial Solar Spectrum, Institute of Environmental Sciences, ISBN 9780915414437, https://books.google.de/books?id=Z4TvAAAAMAAJ, 1973.

380 Dubovik, O., Fuertes, D., Litvinov, P., Lopatin, A., Lapyonok, T., Doubovik, I., Xu, F., Ducos, F., Chen, C., Torres, B., Derimian, Y., Li, L., Herreras-Giralda, M., Herrera, M., Karol, Y., Matar, C., Schuster, G. L., Espinosa, R., Puthukkudy, A., Li, Z., Fischer, J., Preusker, R., Cuesta, J., Kreuter, A., Cede, A., Aspetsberger, M., Marth, D., Bindreiter, L., Hangler, A., Lanzinger, V., Holter, C., and Federspiel, C.: A Comprehensive Description of Multi-Term LSM for Applying Multiple a Priori Constraints in Problems of Atmospheric Remote Sensing: GRASP Algorithm, Concept, and Applications, Frontiers in Remote Sensing, 2, https://doi.org/10.3389/frsen.2021.706851, 2021a.

385 Dubovik, O., Schuster, G. L., Xu, F., Hu, Y., Bösch, H., Landgraf, J., and Li, Z.: Grand Challenges in Satellite Remote Sensing, Frontiers in Remote Sensing, 2, https://doi.org/10.3389/frsen.2021.619818, 2021b.

EUMETSAT: GOME-2 Products Guide; Ref.: EUM/OPS-EPS/MAN/05/0005, Tech. rep., 'https://www-cdn.eumetsat.int/files/2020-04/pdf_man_050005_gome2-pg.pdf', 2005.

EUMETSAT: Validation Report – IASI-A Level 1c FCDR release 1, techreport, EUMETSAT, doc.-No.: EUM/RSP/REP/18/1024768; Issue:
390 v3A e-signed, 2019.

EUMETSAT: GOME-2 Metop-A and -B FDR Product Validation Report Reprocessing R3, techreport, EUMETSAT, doc.-No.: EUM/OPS/-DOC/21/1237264; Issue: v4 e-signed, 2022.

EUMETSAT AC SAF: FOME-2 Instrument, https://acsaf.org/gome-2.php, [Accessed: (08.07.2024)].

European Space Agency: SentiWiki - Sentinel-3 - SLSTR Products, https://sentiwiki.copernicus.eu/web/slstr-products [Accessed:
395 (08.07.2024)], 2024.

Forster, P., Storelvmo, T., Armour, K., Collins, W., Dufresne, J.-L., Frame, D., Lunt, D., Mauritsen, T., Palmer, M., Watanabe, M., Wild, M., and Zhang, H.: The Earth's Energy Budget, Climate Feedbacks and Climate Sensitivity, p. 923–1054, Cambridge University Press, ISBN 9781009157896, https://doi.org/10.1017/9781009157896.002, 2021.

Fougnie, B., Marbach, T., Lacan, A., Lang, R., Schlüssel, P., Poli, G., Munro, R., and Couto, A. B.: The multi-viewing multi-channel
400 multi-polarisation imager – Overview of the 3MI polarimetric mission for aerosol and cloud characterization, Journal of Quantitative Spectroscopy and Radiative Transfer, 219, 23–32, https://doi.org/10.1016/j.jqsrt.2018.07.008, 2018.

Gliß, J., Mortier, A., Schulz, M., Andrews, E., Balkanski, Y., Bauer, S. E., Benedictow, A. M. K., Bian, H., Checa-Garcia, R., Chin, M., Ginoux, P., Griesfeller, J. J., Heckel, A., Kipling, Z., Kirkevåg, A., Kokkola, H., Laj, P., Le Sager, P., Lund, M. T., Lund Myhre, C., Matsui, H., Myhre, G., Neubauer, D., van Noije, T., North, P., Olivié, D. J. L., Rémy, S., Sogacheva, L., Takemura, T., Tsigaridis, K., and
405 Tsyro, S. G.: AeroCom phase III multi-model evaluation of the aerosol life cycle and optical properties using ground- and space-based remote sensing as well as surface in situ observations, Atmospheric Chemistry and Physics, 21, 87–128, https://doi.org/10.5194/acp-21-87-2021, 2021.

Global Modeling And Assimilation Office and Pawson, S.: MERRA-2 inst3_2d_gas_Nx: 2d, 3-Hourly, Instantaneous, Single-Level, Assimilation, Aerosol Optical Depth Analysis V5.12.4, https://doi.org/10.5067/HNGA0EWW0R09, 2015a.

410 Global Modeling And Assimilation Office and Pawson, S.: MERRA-2 inst3_3d_aer_Nv: 3d, 3-Hourly, Instantaneous, Model-Level, Assimilation, Aerosol Mixing Ratio V5.12.4, https://doi.org/10.5067/LTVB4GPCOTK2, 2015b.

Grzegorski, M., Poli, G., Cacciari, A., Jafariserajehlou, S., Holdak, A., Lang, R., Vazquez-Navarro, M., Munro, R., and Fougnie, B.: Multi-Sensor Retrieval of Aerosol Optical Properties for Near-Real-Time Applications Using the Metop Series of Satellites: Concept, Detailed Description, and First Validation, Remote Sensing, 14, 85, https://doi.org/10.3390/rs14010085, 2021.

415 Hasekamp, O. P. and Landgraf, J.: Retrieval of aerosol properties over the ocean from multispectral single-viewing-angle measurements of intensity and polarization: Retrieval approach, information content, and sensitivity study, Journal of Geophysical Research: Atmospheres, 110, https://doi.org/10.1029/2005JD006212, 2005.

Hasekamp, O. P., Landgraf, J., and van Oss, R.: Aerosol retrieval studies for GOME-2, OZONE SAF VISITING SCIENTIST REPORT, 2004.

420 Hébert, P., Blumstein, D., Buil, C., Carlier, T., Chalon, G., Astruc, P., Clauss, A., Siméoni, D., and Tournier, B.: IASI instrument: technical description and measured performances, in: International Conference on Space Optics — ICSO 2004, edited by Costeraste, J. and Armandillo, E., vol. 10568, p. 1056806, International Society for Optics and Photonics, SPIE, https://doi.org/10.1117/12.2308007, 2017.

Holzer-Popp, T. and Schroedter, M.: Retrieval of aerosol properties over land and ocean by exploiting the synergy of GOME and ATSR-2 data, in: IEEE 1999 International Geoscience and Remote Sensing Symposium. IGARSS'99 (Cat. No.99CH36293), vol. 1, pp. 359–361

425 vol.1, https://doi.org/10.1109/IGARSS.1999.773497, 1999.

Holzer-Popp, T., Schroedter-Homscheidt, M., Breitkreuz, H., Martynenko, D., and Klüser, L.: Improvements of synergetic aerosol retrieval for ENVISAT, Atmospheric Chemistry and Physics, 8, 7651–7672, https://doi.org/10.5194/acp-8-7651-2008, 2008.

Holzer-Popp, T., de Leeuw, G., Griesfeller, J., Martynenko, D., Klüser, L., Bevan, S., Davies, W., Ducos, F., Deuzé, J. L., Graigner, R. G., Heckel, A., von Hoyningen-Hüne, W., Kolmonen, P., Litvinov, P., North, P., Poulsen, C. A., Ramon, D., Siddans, R., Sogacheva, L., Tanre,

430 D., Thomas, G. E., Vountas, M., Descloitres, J., Griesfeller, J., Kinne, S., Schulz, M., and Pinnock, S.: Aerosol retrieval experiments in the ESA Aerosol_cci project, Atmospheric Measurement Techniques, 6, 1919–1957, https://doi.org/10.5194/amt-6-1919-2013, 2013.

Hou, W., Wang, J., Xu, X., and Reid, J. S.: An algorithm for hyperspectral remote sensing of aerosols: 2. Information content analysis for aerosol parameters and principal components of surface spectra, Journal of Quantitative Spectroscopy and Radiative Transfer, 192, 14–29, https://doi.org/10.1016/j.jqsrt.2017.01.041, 2017.

435 Hou, W., Li, Z., Wang, J., Xu, X., Goloub, P., and Qie, L.: Improving Remote Sensing of Aerosol Microphysical Properties by Near-Infrared Polarimetric Measurements Over Vegetated Land: Information Content Analysis, Journal of Geophysical Research: Atmospheres, 123, 2215–2243, https://doi.org/10.1002/2017JD027388, 2018.

Inamdar, A. K., Shi, L., Lee, H.-T., Jackson, D. L., and Matthews, J. L.: Extending the HIRS Data Record with IASI Measurements, Remote Sensing, 15, https://doi.org/10.3390/rs15030717, 2023.

440 Kacenelenbogen, M. S. F., Tan, Q., Burton, S. P., Hasekamp, O. P., Froyd, K. D., Shinozuka, Y., Beyersdorf, A. J., Ziemba, L., Thornhill, K. L., Dibb, J. E., Shingler, T., Sorooshian, A., Espinosa, R. W., Martins, V., Jimenez, J. L., Campuzano-Jost, P., Schwarz, J. P., Johnson, M. S., Redemann, J., and Schuster, G. L.: Identifying chemical aerosol signatures using optical suborbital observations: how much can optical properties tell us about aerosol composition?, Atmospheric Chemistry and Physics, 22, 3713–3742, https://doi.org/10.5194/acp-22-3713-2022, 2022.

445 Kaufman, Y. J., Tanré, D., and Boucher, O.: A satellite view of aerosols in the climate system, Nature, 419, 215–223, https://doi.org/10.1038/nature01091, 2002.

Klüser, L., Kleiber, P., Holzer-Popp, T., and Grassian, V.: Desert dust observation from space – Application of measured mineral component infrared extinction spectra, Atmospheric Environment, 54, 419–427, https://doi.org/10.1016/j.atmosenv.2012.02.011, 2012.

Klüser, L., Banks, J., Martynenko, D., Bergemann, C., Brindley, H., and Holzer-Popp, T.: Information content of space-borne
450   hyperspectral infrared observations with respect to mineral dust properties, Remote Sensing of Environment, 156, 294–309, https://doi.org/10.1016/j.rse.2014.09.036, 2015.

Kok, J. F., Storelvmo, T., Karydis, V. A., Adebiyi, A. A., Mahowald, N. M., Evan, A. T., He, C., and Leung, D. M.: Mineral dust aerosol impacts on global climate and climate change, Nature Reviews Earth & Environment, 4, 71–86, https://doi.org/10.1038/s43017-022-00379-5, 2023.

455   Köpke, P.: Satellitenmeteorologie, Ulmer, Stuttgart, ISBN 978-3-8252-3525-3, 2012.

Li, J., Carlson, B. E., Yung, Y. L., Lv, D., Hansen, J., Penner, J. E., Liao, H., Ramaswamy, V., Kahn, R. A., Zhang, P., Dubovik, O., Ding, A., Lacis, A. A., Zhang, L., and Dong, Y.: Scattering and absorbing aerosols in the climate system, Nature Reviews Earth & Environment, 3, 363–379, https://doi.org/10.1038/s43017-022-00296-7, 2022.

Li, L., Dubovik, O., Derimian, Y., Schuster, G. L., Lapyonok, T., Litvinov, P., Ducos, F., Fuertes, D., Chen, C., Li, Z., Lopatin, A., Torres,
460   B., and Che, H.: Retrieval of aerosol components directly from satellite and ground-based measurements, Atmospheric Chemistry and Physics, 19, 13 409–13 443, https://doi.org/10.5194/acp-19-13409-2019, 2019.

Li, L., Che, H., Derimian, Y., Dubovik, O., Schuster, G. L., Chen, C., Li, Q., Wang, Y., Guo, B., and Zhang, X.: Retrievals of fine mode light-absorbing carbonaceous aerosols from POLDER/PARASOL observations over East and South Asia, Remote Sensing of Environment, 247, 111 913, https://doi.org/10.1016/j.rse.2020.111913, 2020.

465   Loyola, D., Erbertseder, T., Balis, D., Lambert, J.-C., Spurr, R., Van Roozendael, M., Valks, P., Zimmer, W., Meyer-Arnek, J., and Lerot, C.: Operational Monitoring of the Antarctic Ozone Hole: Transition from GOME and SCIAMACHY to GOME-2, pp. 213–236, Springer Netherlands, ISBN 9789048124695, https://doi.org/10.1007/978-90-481-2469-5_16, 2009.

Maahn, M., Turner, D. D., Löhnert, U., Posselt, D. J., Ebell, K., Mace, G. G., and Comstock, J. M.: Optimal Estimation Retrievals and Their Uncertainties: What Every Atmospheric Scientist Should Know, Bulletin of the American Meteorological Society, 101, E1512–E1523,
470   https://doi.org/10.1175/BAMS-D-19-0027.1, 2020.

Martynenko, D., Holzer-Popp, T., Elbern, H., and Schroedter-Homscheidt, M.: Understanding the aerosol information content in multi-spectral reflectance measurements using a synergetic retrieval algorithm, Atmospheric Measurement Techniques, 3, 1589–1598, https://doi.org/10.5194/amt-3-1589-2010, 2010.

Matsui, H., Hamilton, D. S., and Mahowald, N. M.: Black carbon radiative effects highly sensitive to emitted particle size when resolving
475   mixing-state diversity, Nature Communications, 9, https://doi.org/10.1038/s41467-018-05635-1, 2018.

Mei, L., Rozanov, V., Rozanov, A., and Burrows, J. P.: SCIATRAN software package (V4.6): update and further development of aerosol, clouds, surface reflectance databases and models, Geoscientific Model Development, 16, 1511–1536, https://doi.org/10.5194/gmd-16-1511-2023, 2023.

Munro, R., Eisinger, M., Anderson, C., Callies, J., Corpaccioli, E., Lang, R., Lefebvre, A., and Livschitz, Y.: GOME-2 on MetOp, Proceedings
480   of The 2006 EUMETSAT Meteorological Satellite Conference, Helsinki, Finland, 1216, 48, 2006.

Munro, R., Lang, R., Klaes, D., Poli, G., Retscher, C., Lindstrot, R., Huckle, R., Lacan, A., Grzegorski, M., Holdak, A., Kokhanovsky, A., Livschitz, J., and Eisinger, M.: The GOME-2 instrument on the Metop series of satellites: instrument design, calibration, and level 1 data processing - an overview, Atmospheric Measurement Techniques, 9, 1279–1301, https://doi.org/10.5194/amt-9-1279-2016, 2016.

Myhre, G., Aas, W., Cherian, R., Collins, W., Faluvegi, G., Flanner, M., Forster, P., Hodnebrog, Ø., Klimont, Z., Lund, M. T., Mülmenstädt,
485   J., Lund Myhre, C., Olivié, D., Prather, M., Quaas, J., Samset, B. H., Schnell, J. L., Schulz, M., Shindell, D., Skeie, R. B., Takemura, T.,
        and Tsyro, S.: Multi-model simulations of aerosol and ozone radiative forcing due to anthropogenic emission changes during the period
        1990–2015, Atmospheric Chemistry and Physics, 17, 2709–2720, https://doi.org/10.5194/acp-17-2709-2017, 2017.

North, P. and Heckel, A.: AOD-SYN Algorithm Theoretical Basis Document, V 1.12, S3-L2-AOD-SYN-ATBD, Swansea Univer-
        sity,   https://sentinels.copernicus.eu/documents/247904/0/SYN_L2-3_ATBD.pdf/8dfd9043-5881-4b38-aae5-86fb9034a94d(lastaccess:
490   9September2022), 2019.

NREL: Solar Spectra - The Thekaekara Spectrum, https://www.nrel.gov/grid/solar-resource/spectra.html, [Accessed: (08.07.2024)].

Popp, T.: Correcting atmospheric masking to retrieve the spectral albedo of land surfaces from satellite measurements, International Journal
        of Remote Sensing, 16, 3483–3508, https://doi.org/10.1080/01431169508954642, 1995.

Randles, C. A., da Silva, A. M., Buchard, V., Colarco, P. R., Darmenov, A., Govindaraju, R., Smirnov, A., Holben, B., Ferrare, R., Hair,
495   J., Shinozuka, Y., and Flynn, C. J.: The MERRA-2 Aerosol Reanalysis, 1980 Onward. Part I: System Description and Data Assimilation
        Evaluation, Journal of Climate, 30, 6823 – 6850, https://doi.org/10.1175/JCLI-D-16-0609.1, 2017.

Rodgers, C. D.: Information content and optimization of high-spectral-resolution measurements, https://doi.org/10.1117/12.256110, 1996.

Rodgers, C. D.: Inverse Methods for atmospheric sounding - Theory and Practice, vol. Vol. 2 of *Series on atmospheric, oceanic and planetary
        physics*, World Scientific, ISBN 981-02-2740-X, 2000.

500 Rozanov, A.: User's Guide for the Software Package SCIATRAN (Radiative Transfer Model and Retrieval Algorithms), Institute of Remote
        Sensing University of Bremen, Germany, 2022.

Rozanov, V., Rozanov, A., Kokhanovsky, A., and Burrows, J.: Radiative transfer through terrestrial atmosphere and ocean: Software package
        SCIATRAN, Journal of Quantitative Spectroscopy and Radiative Transfer, 133, 13–71, https://doi.org/10.1016/j.jqsrt.2013.07.004, 2014.

Samset, B. H., Stjern, C. W., Andrews, E., Kahn, R. A., Myhre, G., Schulz, M., and Schuster, G. L.: Aerosol Absorption: Progress Towards
505   Global and Regional Constraints, Current Climate Change Reports, 4, 65–83, https://doi.org/10.1007/s40641-018-0091-4, 2018.

Sayer, A. M., Thomas, G. E., and Grainger, R. G.: A sea surface reflectance model for (A)ATSR, and application to aerosol retrievals,
        Atmospheric Measurement Techniques, 3, 813–838, https://doi.org/10.5194/amt-3-813-2010, 2010.

Seinfeld, J. H., Bretherton, C., Carslaw, K. S., Coe, H., DeMott, P. J., Dunlea, E. J., Feingold, G., Ghan, S., Guenther, A. B., Kahn, R., Krau-
        cunas, I., Kreidenweis, S. M., Molina, M. J., Nenes, A., Penner, J. E., Prather, K. A., Ramanathan, V., Ramaswamy, V., Rasch, P. J., Ravis-
510   hankara, A. R., Rosenfeld, D., Stephens, G., and Wood, R.: Improving our fundamental understanding of the role of aerosol-cloud interac-
        tions in the climate system, Proceedings of the National Academy of Sciences, 113, 5781–5790, https://doi.org/10.1073/pnas.1514043113,
        2016.

Sherwood, S. C., Bony, S., Boucher, O., Bretherton, C., Forster, P. M., Gregory, J. M., and Stevens, B.: Adjustments in the
        Forcing-Feedback Framework for Understanding Climate Change, Bulletin of the American Meteorological Society, 96, 217–228,
515   https://doi.org/10.1175/bams-d-13-00167.1, 2015.

Simeoni, D., Astruc, P., Miras, D., Alis, C., Andreis, O., Scheidel, D., Degrelle, C., Nicol, P., Bailly, B., Guiard, P., Clauss, A., Blum-
        stein, D., Maciaszek, T., Chalon, G., Carlier, T., and Kayal, G.: Design and development of IASI instrument, in: Infrared Space-
        borne Remote Sensing XII, edited by Strojnik, M., vol. 5543, pp. 208 – 219, International Society for Optics and Photonics, SPIE,
        https://doi.org/10.1117/12.561090, 2004.

520 Sogacheva, L., Kolmonen, P., Virtanen, T. H., Rodriguez, E., Saponaro, G., and de Leeuw, G.: Post-processing to remove residual clouds from aerosol optical depth retrieved using the Advanced Along Track Scanning Radiometer, Atmospheric Measurement Techniques, 10, 491–505, https://doi.org/10.5194/amt-10-491-2017, 2017.

Storelvmo, T.: Aerosol Effects on Climate via Mixed-Phase and Ice Clouds, Annual Review of Earth and Planetary Sciences, 45, 199–222, https://doi.org/10.1146/annurev-earth-060115-012240, 2017.

525 Tilstra, L. G., Tuinder, O. N. E., Wang, P., and Stammes, P.: Surface reflectivity climatologies from UV to NIR determined from Earth observations by GOME-2 and SCIAMACHY, Journal of Geophysical Research: Atmospheres, 122, 4084–4111, https://doi.org/10.1002/2016jd025940, 2017.

Tilstra, L. G., Tuinder, O. N. E., Wang, P., and Stammes, P.: Directionally dependent Lambertian-equivalent reflectivity (DLER) of the Earth's surface measured by the GOME-2 satellite instruments, Atmospheric Measurement Techniques, 14, 4219–4238,
530 https://doi.org/10.5194/amt-14-4219-2021, 2021.

Twomey, S.: Pollution and the planetary albedo, Atmospheric Environment (1967), 8, 1251–1256, https://doi.org/10.1016/0004-6981(74)90004-3, 1974.

Twomey, S.: The Influence of Pollution on the Shortwave Albedo of Clouds, Journal of Atmospheric Sciences, 34, 1149 – 1152, https://doi.org/10.1175/1520-0469(1977)034<1149:TIOPOT>2.0.CO;2, 1977.

535 Vandenbussche, S.: Algorithm Theoretical Basis Document Mineral Aerosol Profiling from Infrared Radiances (MAPIR) Version 4.1b, Tech. rep., Copernicus Climate Change Service, 2021.

Vandenbussche, S., Kochenova, S., Vandaele, A. C., Kumps, N., and De Mazière, M.: Retrieval of desert dust aerosol vertical profiles from IASI measurements in the TIR atmospheric window, Atmospheric Measurement Techniques, 6, 2577–2591, https://doi.org/10.5194/amt-6-2577-2013, 2013.

540 Wiacek, A., Peter, T., and Lohmann, U.: The potential influence of Asian and African mineral dust on ice, mixed-phase and liquid water clouds, Atmospheric Chemistry and Physics, 10, 8649–8667, https://doi.org/10.5194/acp-10-8649-2010, 2010.

Yin, Y., Wurzler, S., Levin, Z., and Reisin, T. G.: Interactions of mineral dust particles and clouds: Effects on precipitation and cloud optical properties, Journal of Geophysical Research: Atmospheres, 107, https://doi.org/10.1029/2001JD001544, 2002.

Zhang, X., Li, L., Chen, C., Chen, X., Dubovik, O., Derimian, Y., Gui, K., Zheng, Y., Zhao, H., Zhang, L., Guo, B., Wang, Y., Holben, B., Che,
545 H., and Zhang, X.: Validation of the aerosol optical property products derived by the GRASP/Component approach from multi-angular polarimetric observations, Atmospheric Research, 263, 105 802, https://doi.org/10.1016/j.atmosres.2021.105802, 2021.

Zhou, D. K., Larar, A. M., Liu, X., Smith, W. L., Strow, L. L., Yang, P., Schlussel, P., and Calbet, X.: Global Land Surface Emissivity Retrieved From Satellite Ultraspectral IR Measurements, IEEE Transactions on Geoscience and Remote Sensing, 49, 1277–1290, https://doi.org/10.1109/TGRS.2010.2051036, 2011.

550 Zhou, D. K., Larar, A. M., and Liu, X.: MetOp-A/IASI Observed Continental Thermal IR Emissivity Variations, IEEE Journal of Selected Topics in Applied Earth Observations and Remote Sensing, 6, 1156–1162, https://doi.org/10.1109/JSTARS.2013.2238892, 2013.

Zhou, D. K., Larar, A. M., and Liu, X.: On the relationship between land surface infrared emissivity and soil moisture, Journal of Applied Remote Sensing, 12, 1, https://doi.org/10.1117/1.jrs.12.016030, 2018.

Zhou, D. K., Larar, A. M., and Liu, X.: Surface Skin Temperature and Its Trend Observations From IASI on Board
555 MetOp Satellites, IEEE Journal of Selected Topics in Applied Earth Observations and Remote Sensing, 14, 1665–1675, https://doi.org/10.1109/JSTARS.2020.3046421, 2021.
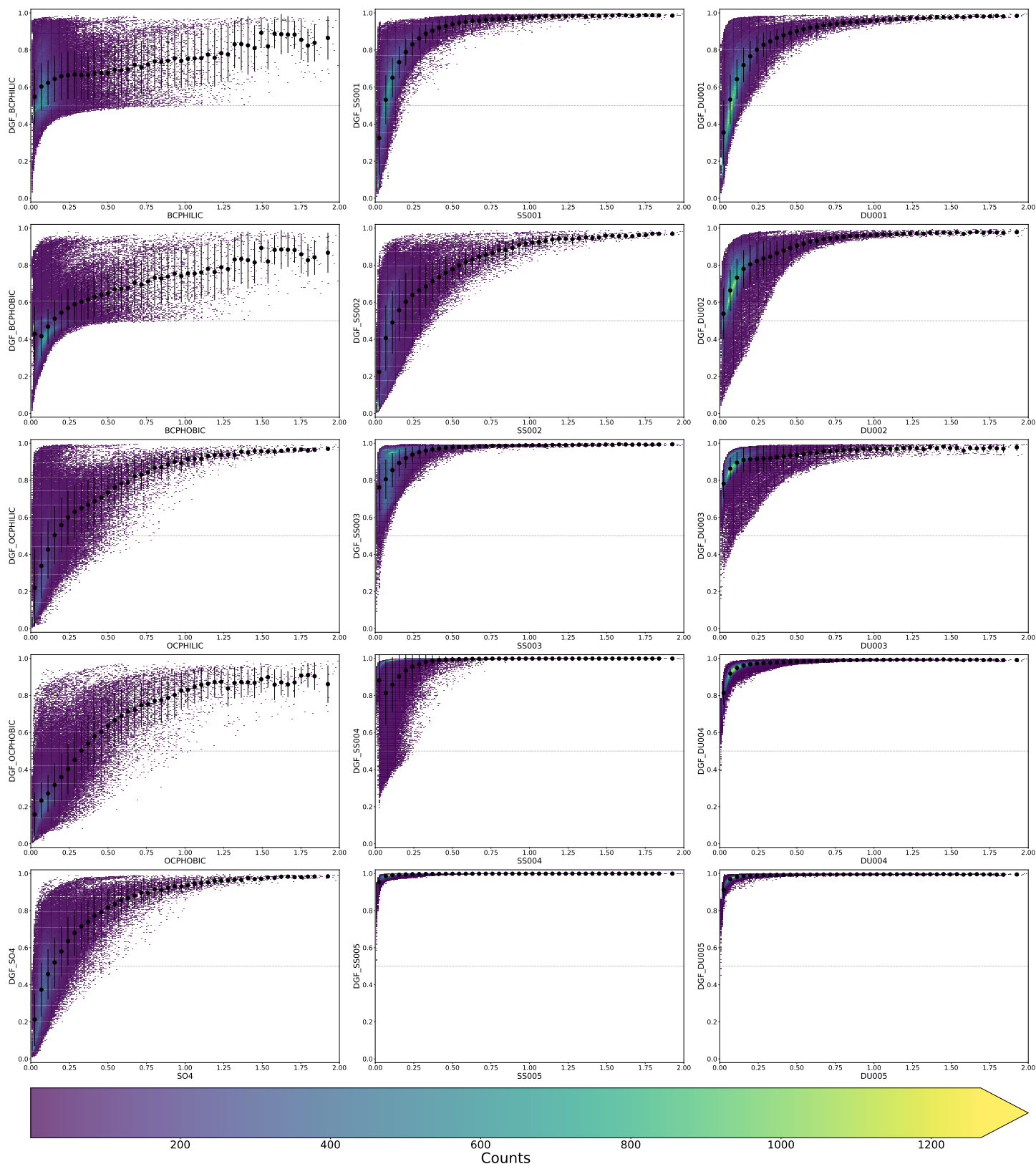
Figure A1. 2D-Histgramms showing the DGF for aerosol components in dependency of the 15 different aerosol components. In addition the binned data is plotted in black (dots for the mean value per bin and error-bar showing the standard deviation) .